J Appl Biotechnol Rep. 2022 June;9(2):582-595

Journal of
Applied Biotechnology Reports

doi 10.30491/JABR.2021.286164.1380

Original Article

Prediction of the Most Deleterious Missense Variants of Human Somatostatin Gene by Combining Computational Algorithms, Molecular Docking and Dynamic Simulations

Mohammed Baqur S. Al-Shuhaib [1*]

[1] Department of Animal Production, College of Agriculture, Al-Qasim Green University, Al-Qasim, Babil 51001, Iraq

Corresponding Author: Mohammed Baqur S. Al-Shuhaib, PhD, Professor, Department of Animal Production, College of Agriculture, Al-Qasim Green University, Al-Qasim, Babil 51001, Tel: +964-7707115693 Iraq. E-mail: mohammed79@agre.uoqasim.edu.iq; baquralhilly_79@yahoo.com

Received May 14, 2021; **Accepted** August 14, 2021; **Online Published** June 18, 2022

Abstract

Introduction: Somatostatin (SST) is a versatile hormone that plays a key role in inhibiting the secretion of several pituitary hormones. It is well known that SST participates in the regulation of other essential proteins throughout the body. The abnormal function of the SST protein is still not fully understood. In this study, the disease susceptible Single Nucleotide Polymorphisms (SNPs) in SST were classified by using different computational algorithms.

Materials and Methods: Sequence-based and structure-based computational tools were employed to classify the most disease susceptible nsSNPs that would have the most harmful effects on SST protein. Docking and molecular dynamic simulations were performed to compare the ability of the normal SST and its most deleterious mutants to bind with corresponding SSTRs to assess the potential role of these nsSNPs to alter protein-protein interactions.

Results: Two nsSNPs, namely L13P, and G104S, were considered to have the most severe functional consequences on the 3D structure of SST. These results were confirmed by molecular dynamic simulations. Docking of SST and its mutant models with SST receptors (SSTR1-SSTR5) showed remarkable roles of both mutant L13P and G104S in altering the binding of SST with SSTR2 and SSTR5.

Conclusions: The findings of the present study provide the first comprehensive *in silico* prediction for assessing the damaging effects of nsSNPs on SST, which may help in a better understanding of how the altered SST would impact the overall health of the body. This study may provide a platform to conduct large-scale experiments on the genetic polymorphism of SST.

Keywords: Prediction, Protein, *In Silico*, SNP, SST, SSTR

Citation: Al-Shuhaib MBS. Prediction of the Most Deleterious Missense Variants of Human Somatostatin Gene by Combining Computational Algorithms, Molecular Docking and Dynamic Simulations. J Appl Biotechnol Rep. 2022;9(2):582-95. doi:10.30491/JABR.2021.286164.1380

Introduction

Somatostatin (SST) is a versatile hormone that is mainly involved in the regulation of nutrients entry from the digestive tract into the blood circulatory system. Since its discovery over more than four decades, the ubiquitous distribution and the multifunctional roles of the SST are still being documented.[1] The broad distribution of SST throughout the body has been widely reported, but it has mainly localized within the central nervous and digestive systems. It has been recognized that this gene acts as the main regulating factor involved in determining the onset of several metabolic pathways. The SST gene has positioned on chromosome 3, within the q27.3. It consists of two exons separated by one intron, with an open reading frame encoding up to 116 amino acids. The pharmacological doses of this hormone have been reported to hinder all gastrointestinal functions by exerting direct effects on the secretion of several crucial hormones in several portions of the body.[2] The SST undergoes a scheduled regulatory task by reducing the concentrations of various hormones that control the rate and storage of glucose, fatty acids, and amino acids in the body, such as insulin and glucagon.[3] Furthermore, the secretions of several gastrointestinal hormones, including gastrin, secretin, Vasoactive Intestinal Polypeptide (VIP), and cholecystokinin, have been shown to be inhibited by SST.[4] The SST has been shown to exert antiproliferative effects on some human tumors via both direct and indirect mechanisms. In addition, the platelets-derived growth factor receptor phosphorylation has been reported to decrease by SST.[5] It's well known that SST participates in endocrine regulation through its binding with a series of cognate somatostatin receptors (SSTR)s, SSTR1 – SSTR5.[6] Actually, SST deficiency has been reported to be associated with the onset of Alzheimer's disease, wherein its concentration has been described to have a considerable reduction in brain tissues. There has been quite lot of evidence revealing that the deficiency of this hormone may have a noticeable

Copyright © 2022 The Author(s). This is an open-access article distributed under the terms of the Creative Commons Attribution License (http://creativecommons.org/licenses/by/4.0), which permits unrestricted use, distribution, and reproduction in any medium, provided the original work is properly cited.

correlation with tumorigenesis.[7,8] However, SST-deficient mice have shown normal growth rates but they have exhibited remarkable elimination of sexually dimorphic liver functions.[9] Recently, several other metabolic disorders have also been associated with dysfunctional SST, such as cardiovascular disease,[10] hypertension,[11,12] vascular dementia,[13] and migraine headache.[14] Thus, most mutations causing a deficiency in SST may damage the vital role played by this hormone in both gastrointestinal and neural activity.[15] Hence, the SNPs observed in the SST can account for susceptibility to various metabolic disorders. The standard protocols for determining the most damaging nsSNPs are time-consuming and expensive. Alternatively, the recent revolution in structural biology has made it possible to develop precise computations to predict the effects of these nonsynonymous Single Nucleotide Polymorphisms (nsSNPs) on the structure of protein, stability, and interactions. Several recent innovations have been utilized to prioritize nsSNPs by providing a cumulative indication for the most deleterious nsSNP on the analyzed protein.[16-18] Despite the main inhibitory role played by SST, no attempt has been made to characterize the most important deleterious effects of its nsSNPs. Therefore, it is crucial to filter out non-deleterious nsSNPs to limit downstream analyses to a handful of candidates of amino acid variations. Taking these data into account, extensive predictions of the effects of nsSNPs on the SST are presented herein with a particular emphasis on the mechanisms of the most harmful nsSNPs in manifesting their deleterious effects on the 3D structure of the SST hormone. Furthermore, molecular dynamic simulation and molecular docking were also used to assess the possible role of the most deleterious SNPs in altering the functions of this essential hormone in the body.

Materials and Methods

Data Retrieval

The corresponding databases for the *SST* gene (Gene ID: 6750) were analyzed following their rsIDs in November 2019. All deposited SNPs were retrieved from the NCBI-dbSNP (https://www.ncbi.nlm.nih.gov/snp/) database. Subsequently, SNPs were verified using the ensemble genome browser 96 (https://asia.ensembl.org/index.html).

Sequence-based Predictions

The effects of the retrieved nsSNPs on the protein structure and biological activity were predicted using 10 major and widely accepted *in silico* tools since the combined effects of these tools would largely improve the prediction accuracy. These tools relied only on the primary sequences of amino acid residues. Accordingly, a cumulative approach was applied for all retrieved nsSNPs to obtain the best possible computations. The potentially deleterious effects of nsSNPs were predicted using Sorting Intolerant From Tolerant (SIFT),[19] Polymorphism Phenotyping (PolyPhen)-2,[20] Rare Exome Variant Ensemble Learner (REVEL),[21] Protein Variation Effect Analyzer (PROVEAN),[22] Protein Analysis Through Evolutionary Relationships (PANTHER),[23] SNAP2 (Predicting Functional Effect of Sequence Variants),[24] PhD SNP (Predictor of Human Deleterious Single Nucleotide Polymorphisms),[25] Mutation Assessor,[26] SUSPect (disease-susceptibility-based SAV phenotype prediction),[27] and UMD-Predictor.[28] The cumulative outcomes of the utilized tools were assessed for each analyzed nsSNP.

Structure-based Predictions

The UniProtKB accession number for SST is P61278, and its NCBI reference sequence is NP_001039.1. The full-length 3-D structure of SST is available in the data deposited in the Protein Data Bank (PDB) server (https://www.rcsb.org/), under the number 1P2W; it covers the entire 116 amino acid residues of the SST protein. The efficiency of the deposited 3D structure of SST was re-evaluated by Qualitative Model Energy Analysis (QMEAN),[29] and by the side chain parameters and Psi/Phi Ramachandran plot of the PROCHECK server.[30] To validate the sequence-based approach, a parallel PDB structure-based approach was also utilized to prioritize all deposited nsSNPs of the *SST* gene. Structure-based predictions were also conducted by 10 well-known *in silico* tools, including I-Mutant2,[31] MAESTRO (Multi Agent Stability Prediction upon Point Mutations),[32] STRUM (STRucture-based stability change prediction Upon single-point Mutation),[33] Mupro,[34] iStable (integrated predictor for Protein Stability change upon single mutation),[35] Cologne University Protein Stability Analysis Tool (CUPSAT),[36] DynaMut,[37] mutation Cut-off Scan Matrix (mCSM),[37] SDM,[38] and DUET.[39]

In-depth Prediction of the Most Damaging nsSNPs

The entirely deleterious nsSNPs in both sequence-based and structure-based, predictions were considered for further downstream analyses, in which the potentials of the mutant SST forms to bind with ligands or receptors were analyzed using several protein-protein and protein-ligand prediction tools. Accordingly, several commonly used tools were utilized to assess the role of these entirely deleterious nsSNPs in altering the binding activity with ligands, proteins, or receptors, including RaptorX,[40] COACH,[41] TM-SITE,[42] COFACTOR,[43] FINDSITE,[44] and ConCavity.[45] The evolutionary conservation grades of these SNPs were analyzed using a Bayesian calculation method by the ConSurf server.[46] To understand the effect of the most damaging SNPs on the 3D structure of SST, site-specific computational mutagenesis was conducted by mutating the native SST with its mutant forms using the Mutate script from the Swiss model PDB viewer tool ver.4.1.0.[47] The normal SST protein and its risky mutants' were superimposed with each other using the Superpose tool.[48] This tool measures the possible differences

in the flexibility of protein structures as revealed by the analysis of variations between different PDB models of the same protein. Afterward, each 3D model was subjected to refinement to remove overhaul distorted geometries using the steepest descent energy minimization provided by Gromacs parameter set.[49] Further in-depth *in silico* analyses were conducted to give further confirmation of the damaging role of both risky nsSNPs on the modeling of the mutant proteins. The modeling and conformational transitions, and the modeling flexibility of normal and mutant protein systems were conducted using the dynamic simulations of the recent release of the CABS-flex 2.0 server.[50] To reveal changes at the atomic level in different time scales for native SST as well as the mutant L13P and G104S complexes, MD simulations were performed using the Nanoscale Molecular Dynamics (NAMD) program.[51] Before starting the simulation, the structures of native and mutant proteins were cleaned, and also the H-bond network was optimized. Then, a cubic cell was formed by extending 6 Å on each side of the protein and a periodic boundary condition was maintained. Configuration files for MD simulations were generated by the CHARMM-GUI web server.[52] All systems were solvated using transferable intermolecular potential water molecules model.[53] MD simulation of each system was run at 310 K to evaluate DIHED (dihedral angles) distortions, and Root Mean Square Deviation (RMSD). Atom trajectories were analyzed using Visual Molecular Dynamic (VMD, ver. 1.9.3).[54] MD simulation files were retrieved from VMD and plotted using Qtgrace visualizer tool ver. 2.6.

Docking

To know the most corresponding receptors for the binding with SST, the String-10 webserver was employed to predict the network interactions between SST and the other proteins in the cell.[55] Then, the currently observed deleterious L13P and G104S nsSNPs may alter these cellular controls by disrupting these variable interactions. Hence, docking experiments of both native and mutant SST forms were performed with those proteins known to be recognized from the SST with the highest affinity. The refined PDB forms of normal SST, as well as its most dangerous mutant forms, were subjected to molecular docking with their substrate using High Ambiguity-Driven Bimolecular Docking (HADDOCK) tool.[56] The default settings of the HADDOCK server were used to dock the wild SST, mutant L13P, and G104S structures against SSTR1-SSTR5. The putative protein-protein interaction sites for SSTR, L13P, G104S, SSTR1, SSTR2, SSTR3, SSTR4, and SSTR5 were determined using the meta server for protein-protein interaction site prediction (meta-PPISP server).[57] The amino acid residues involved in each conducting docking experiment were visualized using PyMol software ver. 7.0.1 (The PyMOL Molecular Graphics System, Schrödinger, LLC.).

Results

Data Retrieval Output

A total of 511 SNPs were retrieved from the NCBI-dbSNP and were verified from the ensemble genome browser 96, including two splice acceptor variants, two stop gained, 84 missense mutations (or nsSNPs), 11 splice region variants, 40 synonymous variants, 51 coding sequence variants, 30 5′ UTR, 42 3′ UTR, and 249 intronic variants (Figure 1A). All of the retrieved 84 nsSNPs of the SST protein were selected for the downstream *in silico* predictions.

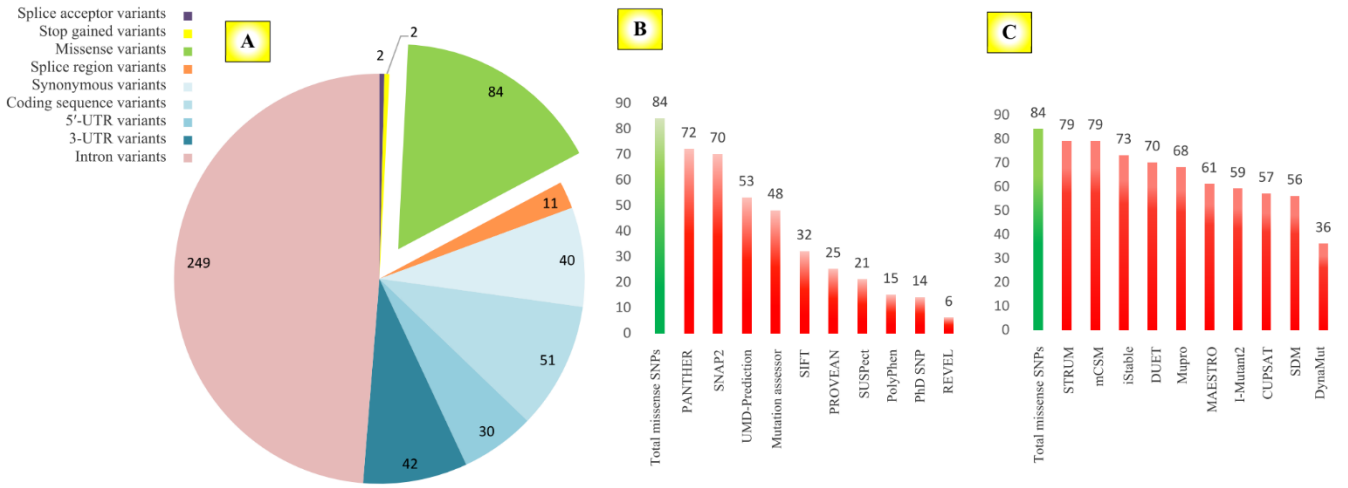

Figure 1. Distribution and Description of All Single-nucleotide Polymorphisms (SNPs) in *SST* Gene, Including Splice Acceptor, Stop Gained, Missense, Splice Region, Synonymous, Coding Sequence, 5′-UTR, 3′-UTR, and Introns Variants **(a)**. The number of predicted damaging non-synonymous SNPs (nsSNPs) in the *SST* gene by 10 different sequence-based *in silico* tools **(b)**. The number of predicted damaging nsSNPs in *SST* gene by 10 different structure-based *in silico* tools **(c)**. The green color refers to nsSNPs, while the red color indicates the damaging effects of nsSNPs predicted by state-of-the-art *in silico* tools.

Table 1. Cumulative Predictions for the Entirely Deleterious Nonsynonymous SNPs of SST Protein as Seen by 20 *in silico* Tools. **A)** sequence-based prediction made by ten *in silico* tools. **B)** structure-based prediction made by ten *in silico* tools. prediction values were calculated using DDG values, which presented to indicate free energy change upon mutation

A) Sequence-based prediction											
Variant ID	**mutation**	**SIFT**	**PolyPhen**	**REVEL**	**PROVEAN**	**PANTHER**	**SNAP2**	**PhD SNP**	**Mutation assessor**	**SUSPect**	**UMD-Predictor**
rs1250282492	L13P	0	0.997	0.604	-4.505	456	76	7	0.789	92	84
rs778060901	G104S	0.01	0.999	0.579	-4.032	456	69	4	0.694	91	84
B) Structure-based prediction											
Variant ID	**mutation**	**I-Mutant2**	**MAESTRO**	**STRUM**	**Mupro**	**iStable**	**CUPSAT**	**DynaMut**	**mCSM**	**SDM**	**DUET**
rs1250282492	L13P	-1.81	1.913	-1.81	-1	-2.27	-1.44	-1.588	-1.494	-2.23	-1.853
rs778060901	G104S	-0.84	0.950	-1.68	-1	-0.71	-1.48	-0.518	-1.152	-3.08	-1.489

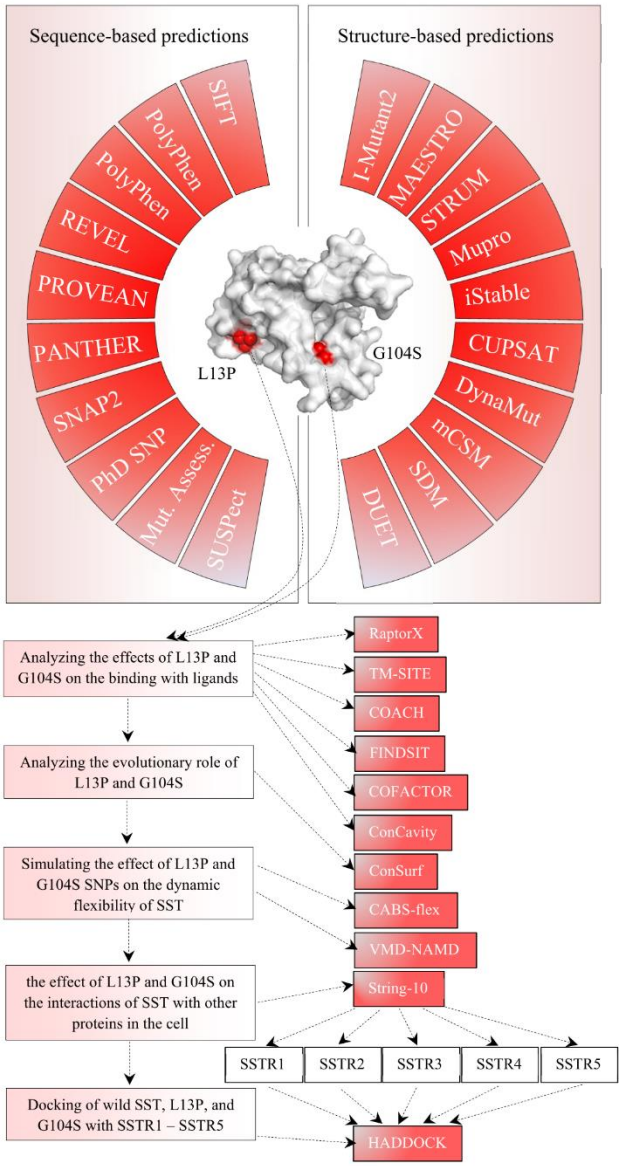

Figure 2. A Schematic Diagram for the Entire Study, in Which the Most Deleterious Nonsynonymous SNPs (nsSNPs) on Somatostatin Were Predicted and Shown as Red Bulls Within a Transparent Surface View of Somatostatin.

Sequence-based Predictions

A total of 10 different *in silico* tools were utilized to predict the deleterious nsSNPs using the primary amino acid sequences of the SST, including SIFT, PolyPhen, REVEL, PROVEAN, PANTHER, SNAP2, PhD SNP, Mutation Assessor, SUSPect, and UMD-Predictor. Cumulative results concerned with the prediction of nsSNPs consequences indicated a concordant deleterious effect for two nsSNPs, including L13P and G104S on SST structure and biological activity (Table 1). However, this study was only concerned with the entirely deleterious nsSNPs. Thus, other deleterious SNPs that did not exhibit a concordant deleterious effect were eliminated from further analyses (Suppl. Table 1). Out of the 84 nsSNPs, the total number of damaging nsSNPs reported from all tools were described, in which Panther and STRUM predicted the highest number of deleterious SNPs among all sequence-based and structure-based *in silico* tools, respectively (Figure 1, B and C).

Structure-based Predictions

The effects of nsSNPs on protein structure, function, and stability were also analyzed by another set of 10 computational tools based on the PDB-based 3D structures of SST, including I-Mutant2, MAESTRO, STRUM, Mupro, iStable, CUPSAT, DynaMut, mCSM, SDM, and DUET. Cumulative results indicated concordant deleterious effects of seven nsSNPs, including L13P, L13V, I15T, I15F, V16A, V22A, A25S, R30G, L31P, R32G, F34V, A43T, E47G, A49S, and A54G (Suppl. Table 2). Thus, both sequence-based and structure-based predictions revealed concordant deleterious effects of only two nsSNPs, namely L13P and G104S (Figure 2).

In-depth Analyses of the Entirely Damaging SNPs

Further analyses were conducted on the most deleterious L13P and G104S nsSNPs to explore the pattern of each one to cause such drastic alteration in the mutant SST protein. The conducted ConSurf results revealed a higher conserved status of G-104 residue over L-13 residue (Figure 3). Moreover, a dynamic role was revealed from G-104 residue since it was located in a functional-exposed portion as it was predicted from the neural network-based ConSurf tool. Further details were provided from the 3D of SST. The main functional domains in the 3D structure of SST were highlighted starting from N-terminal to C-terminal, including a signal peptide, neurostatin, propeptide, somatostatin-28, and somatostatin 14 (Figure 4). From this tertiary structure, it was shown that L13P and G104S were resided in the signal

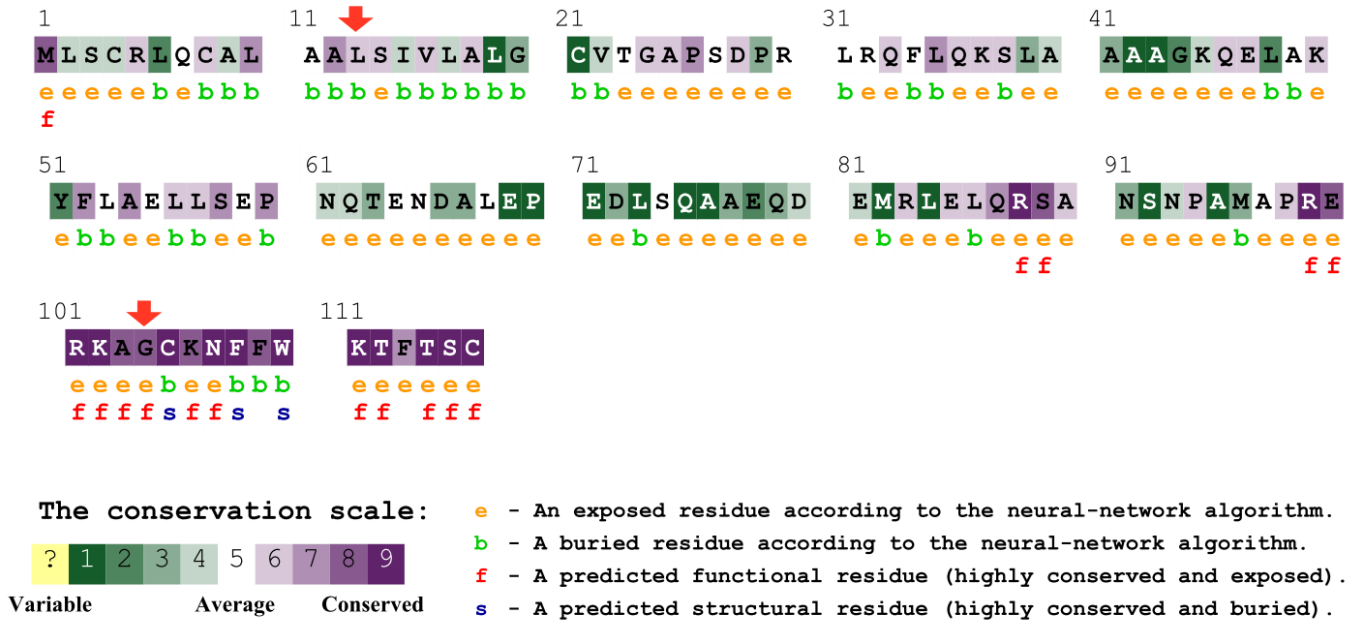

Figure 3. The Evolutionary Conservative Positioning of the Most Deleterious Nonsynonymous SNPs (nsSNPs), L13P and G104S, Identified in Somatostatin. The grade of the conservation pattern of both amino acid residues is highlighted within the primary sequence of the wild-type somatostatin. Color intensity increases with the degree of conservation. The amino acids are colored based on their conservation grades and conservation levels. The amino acid positions of the most two deleterious nsSNPs are indicated by red arrows.

peptide and somatostatin-14, respectively. The nature of the polar interactions of the observed most deleterious L13P and G104S nsSNPs observed in the signal peptide and somatostatin-14 regions was tested by PyMol to understand their potential participation in the conversion of the native amino acid binding with its surrounding residues. A substantial alteration in electrostatic interactions was seen in the SST upon mutation with both L13P and G104-S (Figure 5, A and B).

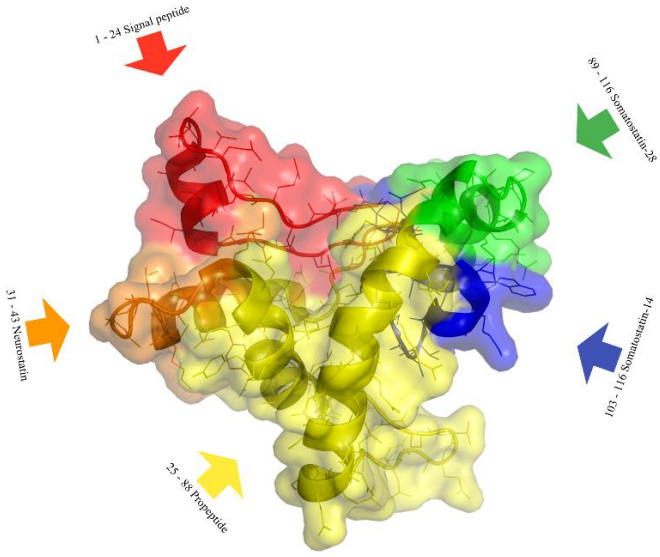

Figure 4. The Main Functional Domains Within Somatostatin Within a Transparent Surface View of Somatostatin. Five domains are highlighted in somatostatin 3-dimensional structure, including signal peptide (red), propeptide (yellow), neurostatin (orange), somatostatin-28 (green), and somatostatin-14 (blue).

Concerning G104S, it was found that the Gly-104 residue had one polar interaction with Glu-100 residue, of 3.0 Å length, in the native SST protein, while Ser-104 residue formed two extra polar interactions with Lys-102 residue, of 3.4 Å length, in the altered SST form. Considering L13P, the amino acid residue Leu-13 exerted no polar interaction with any other residues in the native SST, while Pro-13 residue formed one polar interaction with the surrounding Leu-10 residue, of 3.4 Å length, in the mutant SST form. Results showed no post-translational effects for both L13P and G104S nsSNPs. The possibility of these highly risky nsSNPs to alter the binding activity with other proteins was analyzed by utilizing seven prediction tools, namely RaptorX, COACH, TM-SITE, S-SITE, COFACTOR, FINDSITE, and ConCavity. The FINDSITE tool indicated the obvious involvement of G104S in the alteration of the binding activity of the mutant SST with receptors (Table 2). The conducted superimposition of the native SST and its two mutant models indicated very close homology between the native template and both models (Figure 6). This observation revealed a fair superimposition of the native SST with its two mutant forms. The total energy values for the native SST structure and the two mutant modeled L13P and G104S structures were -1849.877, -1778.814, and -1901.481 KJ/mol, respectively. L13P showed a noticeable increase in energy than the native structure. These less favorable changes indicated a more deleterious nature of the L13P model than the G104S model in inducing broader structural instability in the altered G104S SST form than the L13P SST form. Further analyses were performed to assess

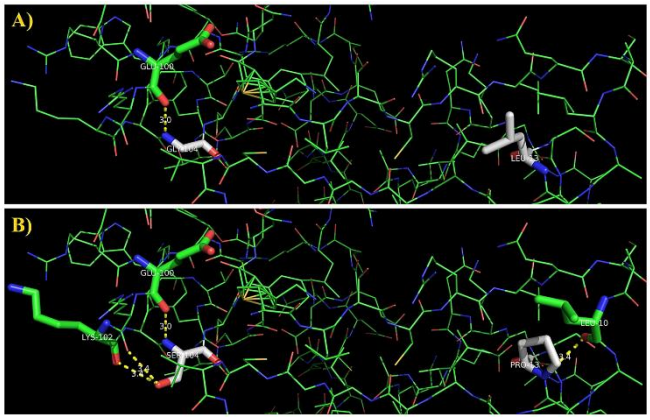

Figure 5. The Alteration in Polar Interactions of the Native Somatostatin and Its L13P and G104S Mutant Forms, in Terms of the Most Deleterious Amino Acid Residues with Vicinal Units Before and After Mutation. **A)** Native somatostatin, in which no polar interaction was observed in Leu (L)-13 residue, while only one polar interaction with Glu-100 was observed with Leu-104. **B)** Mutant somatostatin, in which one polar interaction between Pro-13 and Leu-10 was seen, while two interactions were observed between the mutant Ser-104 and both Glu-100 and Lys-102. The connection (yellow dotted lines) lengths between residues were measured in Å dimensions.

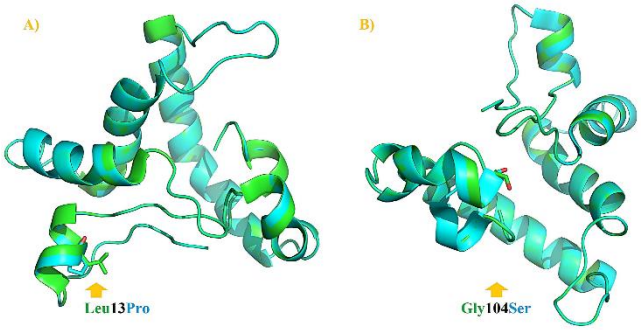

Figure 6. Spatial Superimposition of the Native Somatostatin and The Most Deleterious Mutants Predicted in This Study. 3D model of native somatostatin superimposed and its mutant protein having a mutation from Leu(L) to Pro(P) at 13th position and from Gly(G) to Ser(S) at 104th position in (a) and (b) respectively. The green and blue colors refer to wild-type and mutant forms, respectively. Superimposition was viewed by PyMol software.

the overall effect of each identified deleterious nsSNP on the 3D modeling of the SST structure flexibility. The damaging effects of L13P and G104S models were further demonstrated by comparing the RMSF peaks for normal and mutant SST models. Results of dynamic simulation, flexibility, structural clustering, and dynamic protein fluctuations differences between normal and mutant models provided additional proof for the ability of L13P and G104S SNPs to damage the 3D structure of the SST protein (Figure 7).

A comparative MD analysis of the predicted deleterious mutants L13P and G104S with the native SST was carried out. In the conducted simulation trajectory, two different parameters were applied to analyze the level of structural changes in these models by using different parameters, namely

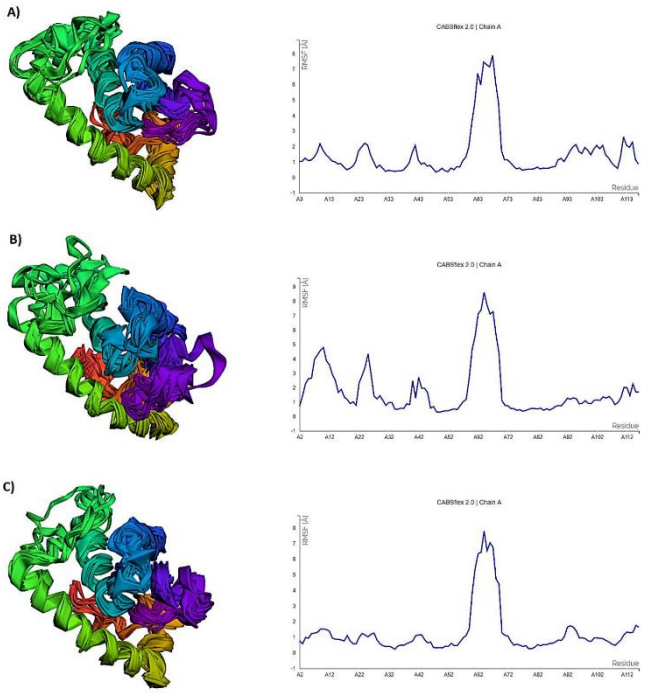

Figure 7. Aggregation Propensity Simulation and Fluctuation Plots for the Wild-type SST and Its Deleterious Models. **A)** Wild-type SST protein. **B** and **C)** Deleterious L13P and G104S models. RMSF: Root mean square fluctuation.

bond, angle, DIHED, and RMSD. The DIHED analysis based on MD trajectories showed a respective higher deviation for G104S and L13P than that found in the wild SST. This observation entailed the possible participation of G104S, and with a little extent L13P, in inducing a conformational change in the SST 3D structure (Figure 8A). Further confirmation was observed from RMSD calculations that showed that the mutant G104S had exhibited a remarkable deviation in the backbone RMSD than that found in L13P and the wild SST respectively in almost all conducted simulation times (Figure 8B).

Docking with Somatostatin Receptors

String 10 server showed that SST mainly interacts with a variety of cognate SST-receptors, including SSTR1-SSTR5, which mainly participate in the control of several metabolic events in the cell (Figure 9). Subsequently, the molecular docking between the normal SST and its two risky mutant forms with SSTRs (SSTR1-SSTR5) was performed to identify the extent of variation in the overall SST-SSTR interaction energy before and upon mutation. Using the RaptorX tool,[40] five 3D models were generated to represent SSTR1-SSTR5, respectively. However, the docking of this specified SSTRs molecule with SST protein indicated a clear role of the L13P and G104S in inducing a remarkable change in the binding with SSTR2 and SSTR5, while less dramatic effects were observed in the binding with SSTR1, SSTR4, and SSTR3 respectively (Table 3). Compared with

Table 2. The Mechanisms of Deleterious Effects of the Most Damaging Missense SNPs of Somatostatin. A) Post-translation modification prediction, B) receptor binding prediction. Symbols phos., ubi., meth., SUMO., O-GalNAc., O-GlcNAc., N-Gly., K-Ace., N-t-ace. refer to phosphorylation, ubiquitination, methylation, sumolation, *O*-*N*-acetylgalactosamination, *O*-*N*-acetylglucosamination, *N*-glycosylation, *K*-acetylation, *N*-*t*-acetylation respectively

SNP	Amino acid correspondence	Altered binding with ligands/receptors upon mutation						
		RaptorX	COACH	TM-SITE	S-SITE	COFACTOR	FINDSITE	ConCavity
rs1250282492	L13P	-	-	-	-	-	-	-
rs778060901	G104S	-	-	0.13*	-	-	-	-

* C-score is the confidence score of predicted binding site. C-score ranges [0-1], where a higher score indicates a more reliable prediction

Table 3. Molecular Docking Differences Between the Native and Two Risky Mutant Forms of SST as Determined by the HADDOCK Webserver

Protein-protein interaction	HADDOCK score	Cluster size	RMSD from the overall lowest-energy structure	Van der Waals energy	Electrostatic energy	Desolvation energy	Restraints violation energy	Buried Surface Area	Z-Score
SST-SSTR1	-50.6 +/- 9.1	185	1.1 +/- 1.0	-74.8 +/- 7.0	-40.3 +/- 15.5	-22.0 +/- 1.5	542.3 +/- 61.1	2556.2 +/- 138.1	-1.3
L13P-SSTR1	-52.2 +/- 8.2	183	1.1 +/- 1.0	-75.9 +/- 5.7	-42.5 +/- 13.2	-21.2 +/- 2.7	534.5 +/- 70.7	2564.2 +/- 124.3	-1.3
G104S-SSTR1	-44.9 +/- 8.2	186	1.3 +/- 1.1	-69.7 +/- 7.3	-31.9 +/- 11.0	-21.5 +/- 1.9	526.4 +/- 65.7	2479.3 +/- 151.3	-1.3
SST-SSTR2	-59.5 +/- 5.9	19	11.0 +/- 0.1	-55.1 +/- 6.8	-449.4 +/- 62.9	-13.0 +/- 14.0	984.2 +/- 70.9	2547.1 +/- 143.6	-1.4
L13P-SSTR2	-54.7 +/- 8.9	12	0.7 +/- 0.5	-58.0 +/- 3.9	-315.9 +/- 11.5	-23.0 +/- 3.0	895.0 +/- 89.9	2403.5 +/- 57.0	-1.6
G104S-SSTR2	-38.1 +/- 8.3	49	0.8 +/- 0.6	-78.4 +/- 10.6	-252.2 +/- 70.1	-4.1 +/- 2.6	948.9 +/- 106.1	2670.5 +/- 96.0	-2.3
SST-SSTR3	115.7 +/- 6.2	16	14.3 +/- 0.0	-78.7 +/- 3.4	-124.7 +/- 29.6	-10.3 +/- 1.5	2296.1 +/- 58.5	2732.7 +/- 37.8	-1.6
L13P-SSTR3	105.3 +/- 9.8	10	0.5 +/- 0.3	-92.8 +/- 5.6	-94.2 +/- 20.0	-12.8 +/- 2.4	2296.4 +/- 139.0	2941.4 +/- 110.1	-1.6
G104S-SSTR3	100.8 +/- 19.8	16	0.6 +/- 0.4	-69.1 +/- 4.7	-157.0 +/- 35.6	-14.3 +/- 2.4	2156.7 +/- 204.9	2755.4 +/- 44.4	-1.5
SST-SSTR4	20.4 +/- 2.8	46	0.6 +/- 0.4	-69.7 +/- 7.2	-126.1 +/- 45.9	-24.0 +/- 4.9	1393.6 +/- 110.1	2601.5 +/- 121.1	-1.7
L13P-SSTR4	8.2 +/- 9.4	22	0.5 +/- 0.3	-65.7 +/- 3.4	-155.5 +/- 14.5	-22.9 +/- 4.1	1278.0 +/- 27.3	2557.9 +/- 25.5	-2.1
G104S-SSTR4	12.4 +/- 7.4	34	0.4 +/- 0.2	-65.5 +/- 2.6	-161.6 +/- 12.2	-24.9 +/- 2.4	1351.9 +/- 73.5	2592.3 +/- 50.8	-1.9
SST-SSTR5	45.8 +/- 10.2	5	3.5 +/- 0.4	-64.6 +/- 2.6	-60.5 +/- 14.7	-30.8 +/- 1.6	1534.1 +/- 98.3	2570.8 +/- 116.9	-1.8
L13P-SSTR5	29.4 +/- 13.7	17	1.0 +/- 1.0	-70.1 +/- 6.8	-62.2 +/- 16.5	-25.2 +/- 2.8	1371.0 +/- 99.5	2587.5 +/- 58.2	-1.4
G104S-SSTR5	34.4 +/- 30.9	4	0.6 +/- 0.3	-79.5 +/- 12.2	-90.0 +/- 27.1	-27.0 +/- 1.9	1588.3 +/- 154.8	3218.9 +/- 75.6	-1.4

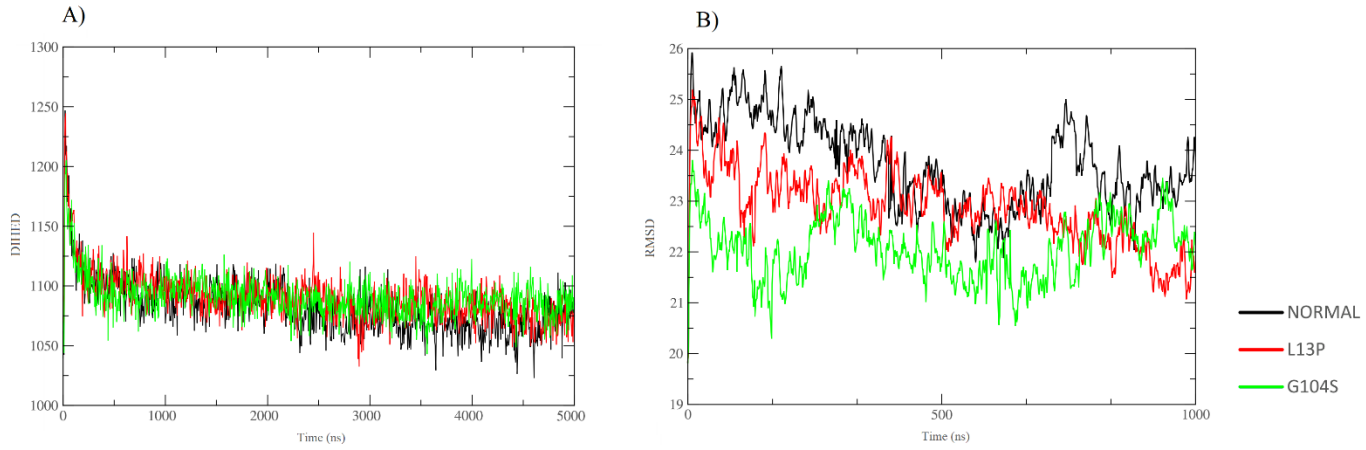

Figure 8. Molecular Dynamic Simulations of the Wild SST, Mutant L13P, and G104S on SST Protein. **A)** Dihedral angle distortion (DIHED) of the three models in 5000 ns. **B)** Root mean square deviation (RMSD) of the three models in 1000 ns. The symbol coding scheme is as follows: native (black colour), mutant L13P (red colour), and G104S (green colour).

the wild SST-SSTR1 (Figure 10A), only a slight contribution of L13P was seen in the docking against SSTR1 because no substantial conformational changes were observed in this complex than that found in the docking of the wild SST with SSTR1 (Figure 10B). However, fewer amino acid residues were involved in L13P-SSTR1 compared with the wild SST-SSTR1. The same thing was also observed in the case of G104S-SSTR1 with slight alterations in amino acid interactions (Figure 10C). Concerning SSTR2, noticeable alterations were observed in the docking of SSTR2 against the wild SST (Figure 11A), L13P (Figure 11B), and G104S (Figure 11C). Interestingly, L13P exerted more conformational

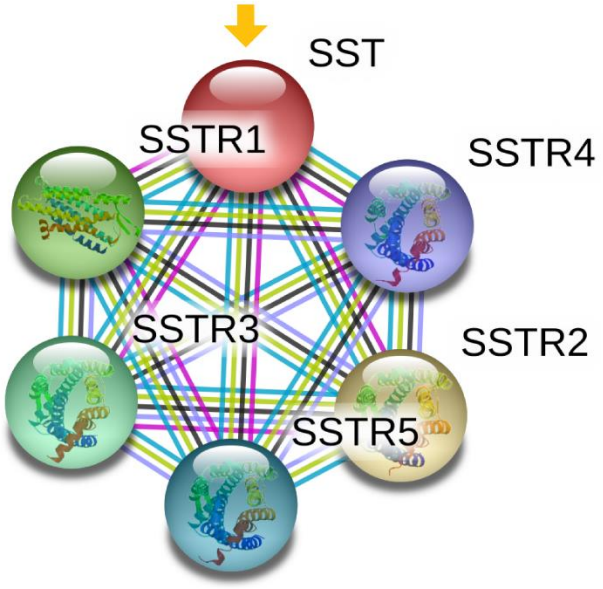

Figure 9. The Functional Association Network of the Somatostatin (SST) With Its Corresponding Receptors (SSTRs) in the Cellular Metabolic System. The predicted protein-protein interaction network is represented with variable extending threads. The color of these threads refers to the intensity of binding between somatostatin and its five (SSTR1-SSTR5) receptors. The yellow arrow refers to the targeted somatostatin protein.

changes than that observed in G104S. Concerning docking of SSTs-SSTR3, results showed moderate alterations among SST-SSTR3 (Figure 12A), L13P-SSTR3 (Figure 12B), and G104S-SSSTR3 (Figure 12C). As in the case of SSTR2, docking of L13P-SSTR3 exhibited more conformational changes than that observed in G104S. However, the amino acid residues involved in G104S-SSTR3 were less than those contributed in L13P-SSTR3 and SST-SSTR3 respectively. Concerning SSTR4, no remarkable conformational differences were observed in the docking of SSTR4 against the wild SST (Figure 13A), L13P (Figure 13B), and G104S (Figure 13C). However, higher amino acid interactions were involved in both L13P-SSTR4 and G104S-SSTR4 compared with the wild SST-SSTR4. Another remarkable binding alteration was also observed in the binding of these three models with SSTR5 (Figure 14A-C). Both L13P and G104S exerted a noticeable binding alteration with SSTR5 compared to what was observed in the native SST. These differences were observed in the presence of obvious alterations in 3D conformations and the number of amino acid residues involved in these docking experiments.

Discussion

The current study used many computational tools based on the variable of algorithms to prioritize the most dangerous amino acid substitutions on the SST protein. The number of nsSNPs highly exceeded the number of SNPs detected in the untranslated regions. This observation indicates the crucial importance of these amino acid substitutions in acting on the structure of the *SST* gene products. Hence, the necessity to determine whether each nsSNP having neutral or deleterious consequences is mandatory to be prioritized by the available tools. To be a damaging missense SNP for a particular amino acid, it must be validated by at least four *in silico* tools usually used in SNP Prediction.[58,59] Accordingly, the retrieved nsSNPs were extensively analyzed to assess their

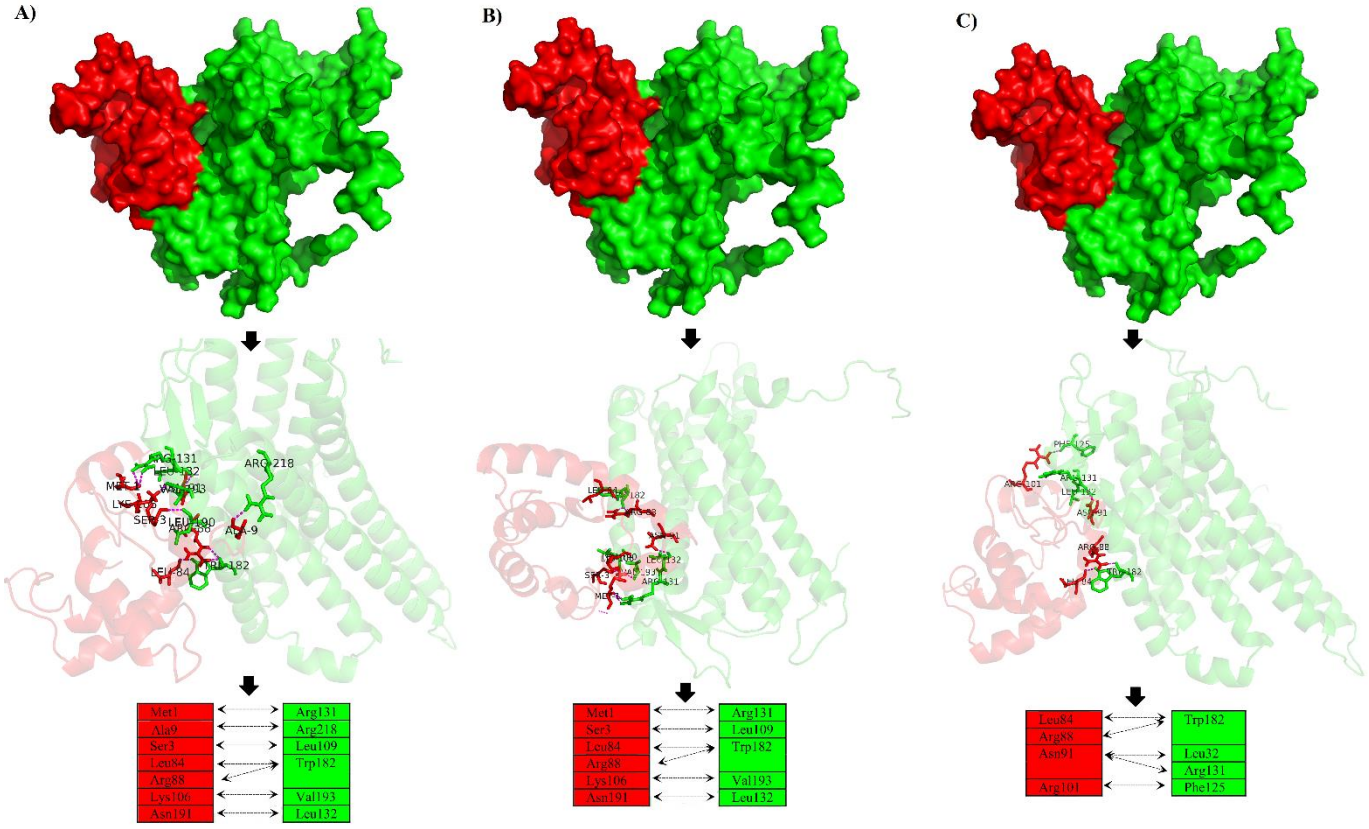

Figure 10. The Comparative Docking Views for the Binding of the Native Somatostatin and Its Highly Damaging Mutant Forms of L13P and G104S with Somatostatin Receptor 1 (SSTR1) Substrate. **A)** docking view of the wild SST with SSTR1. **B)** Alteration in docking view of the mutant L13P SST with SSTR1. **C)** Alteration in docking view of the mutant G104S SST with SSTR1. SST and SSTR1 are denoted in red and green, respectively.

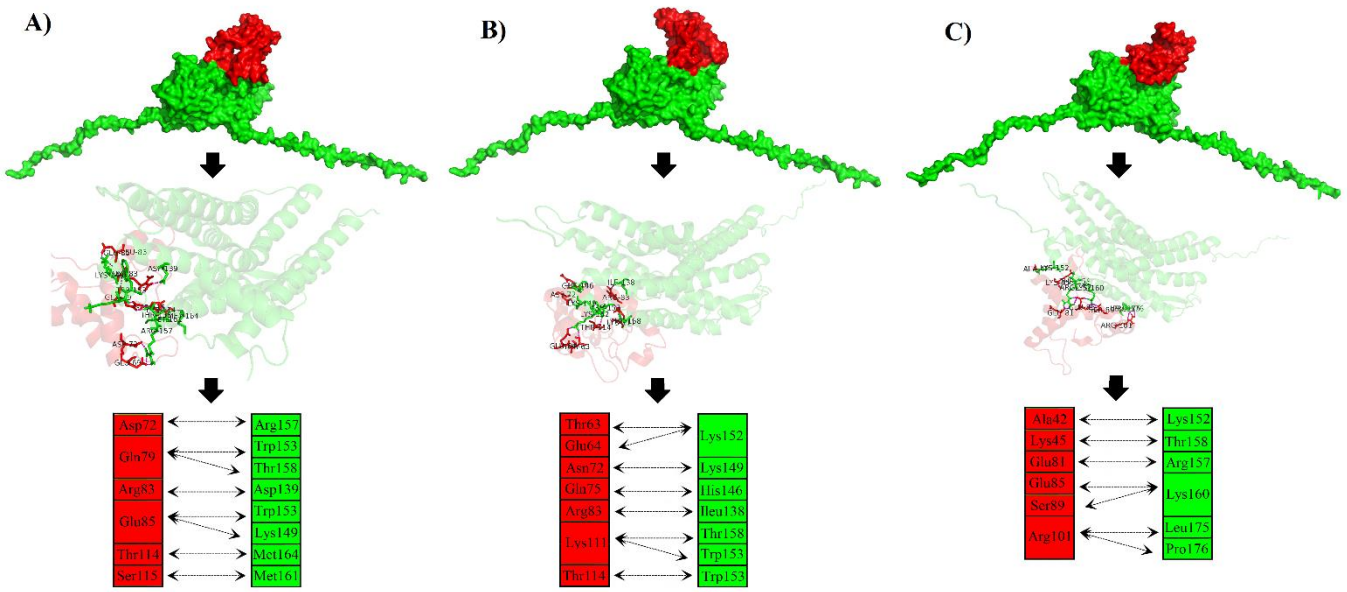

Figure 11. The Comparative Docking Views for the Binding of the Native Somatostatin and Its Highly Damaging Mutant Forms of L13P and G104S with Somatostatin Receptor 2 (SSTR2). **A)** docking view of the wild SST with SSTR2. **B)** Alteration in docking view of the mutant L13P SST with SSTR2. **C)** Alteration in docking view of the mutant G104S SST with SSTR2. SST and SSTR2 and their amino acid interactions are denoted in red and green, respectively.

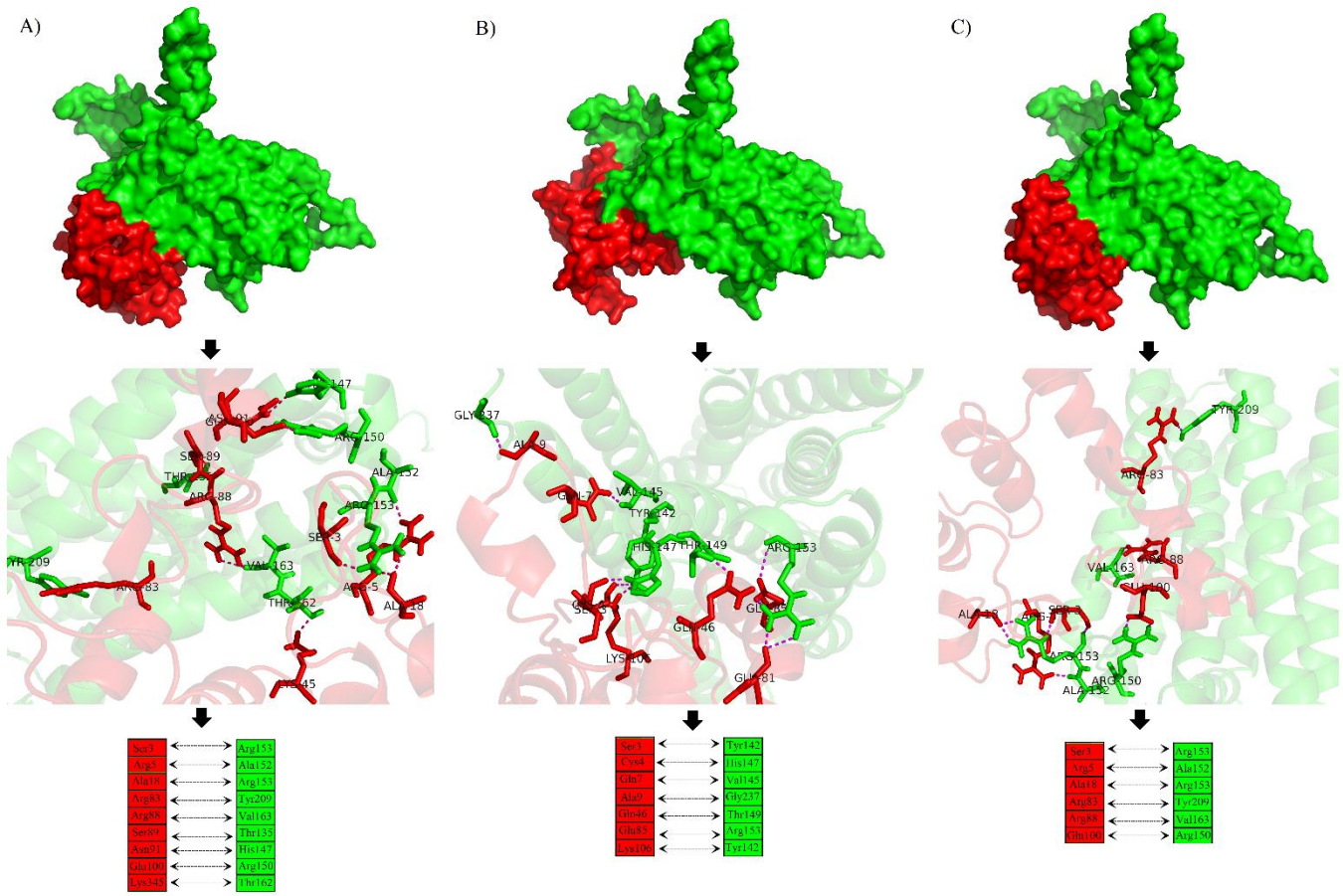

Figure 12. The Comparative Docking Views for the Binding of the Native Somatostatin and Its Highly Damaging Mutant Forms of L13P and G104S with Somatostatin Receptor 3 (SSTR3). **A)** docking view of the wild SST with SSTR3. **B)** Alteration in docking view of the mutant L13P SST with SSTR3. **C)** Alteration in docking view of the mutant G104S SST with SSTR3. SST and SSTR3 and their amino acid interactions are denoted in red and green, respectively.

cumulative effects on structure, function, and stability. Though sequence-based prediction tools are working on diverse principles, they only require amino acid residues in a FASTA format as the input sequence. Whereas the tertiary structure represented by the PDB file is extremely mandatory as an input template for structure-based prediction tools.[60] Based on both approaches, two SNPs, L13P (rs1250282492) and G104S (rs778060901), were disclosed with completely deleterious consequences on protein structure, function, and stability. For this reason, it is necessary to understand the mechanisms through which each risky SNP is relied on to undertake its scheduled damaging role on SST. Add to that, further in-depth analyses were utilized to apprehend how such SNPs affect the interaction of other proteins in the metabolic pathways in which SST is being involved.

The higher degree of evolutionary conservation of L-13 and G-104 residues may justify some of their serious contributions in damaging SST. However, the evolutionary conservation results indicated a more dynamic role for G-104 in disrupting SST. This is due to the highly functionally conserved positioning of G-104 in the primary structure of SST than the buried and less conservative position occupied by L-13. The highly dynamic role of G104S was also confirmed by the analysis of 3D structure due to its distinctive position within the somatostatin-14 domain. Whereas L-13 residue was located in the SST signal portion that may take a different role in the SST mode of action.

More confirmation for the dramatic changes played by G104S over L13P was revealed from the nature of polar interactions. The substitution of non-polar Gly-104 to the polar Ser-104 may lie behind the substantial alteration detected in the mutant G104S. However, the conversion of the non-aromatic Leu-13 to the aromatic Pro-13 was also crucial to SST functions.

To further evaluate our hypothesis as to whether L13P and G104S mutants have a deleterious effect on SST protein, MD simulation analysis was performed to observe the effect of each mutation on the structural dynamics of the SST protein. It was inferred from RMSD values that both G104S and L13P mutants were very unstable from the beginning of the simulation over the period of 1000 ns. The higher fluctuation and the loss of stability might be explained in terms of the structural differences in the amino acid backbone in both observed mutations, which referred to

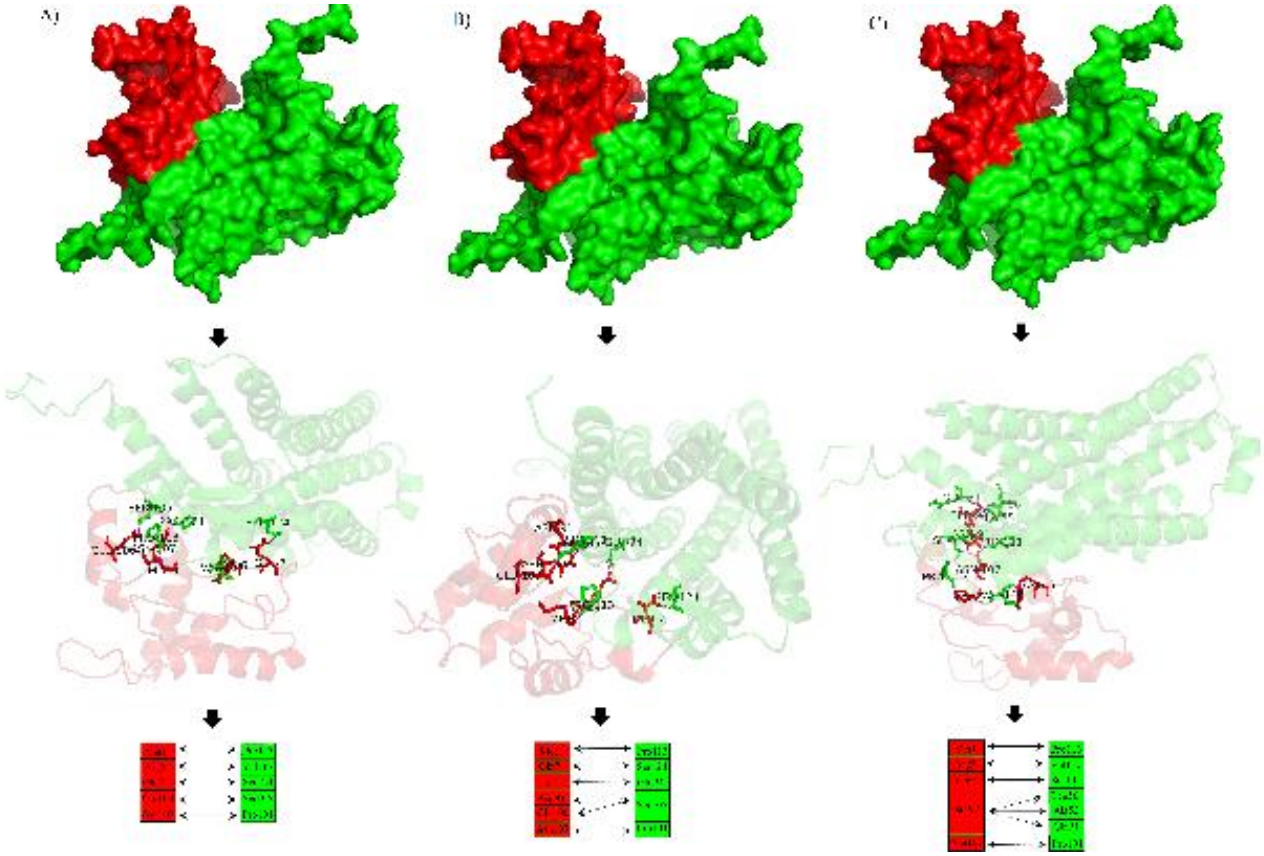

Figure 13. The Comparative Docking Views for the Binding of the Native Somatostatin and Its Highly Damaging Mutant Forms of L13P and G104S with Somatostatin Receptor 4 (SSTR4). **A)** docking view of the wild SST with SSTR4. **B)** Alteration in docking view of the mutant L13P SST with SSTR4. **C)** Alteration in docking view of the mutant G104S SST with SSTR4. SST and SSTR4 and their amino acid interactions are denoted in red and green, respectively.

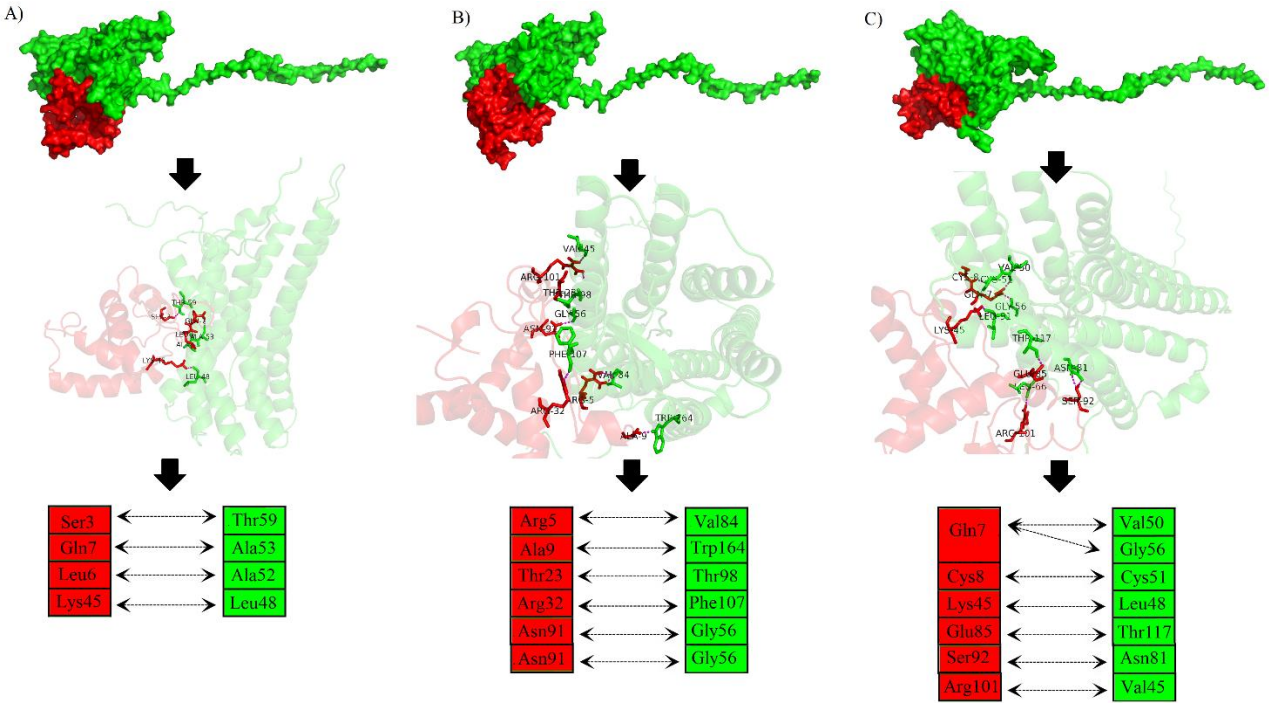

Figure 14. The Comparative Docking Views for the Binding of the Native Somatostatin and Its Highly Damaging Mutant Forms of L13P and G104S with Somatostatin Receptor 5 (SSTR5). **A)** docking view of the wild SST with SSTR5. **B)** Alteration in docking view of the mutant L13P SST with SSTR5. **C)** Alteration in docking view of the mutant G104S SST with 5 SST and SSTR5 and their amino acid interactions are denoted in red and green, respectively.

significant structure transitions when compared to the native SST structure.

In addition to MD simulation, it is mandatory to investigate the role of both nsSNPs in inducing any possible interruption with respect to SST binding with its cognate SSTRs. Docking experiments were performed between the tertiary structures of normal SST and its deleterious mutants with all five SSTRs. Though no significant contribution of L13P and G104S was observed in changing SST binding with SSTR1, SSTR3, and SSTR4, a clear conformational change was proven in the binding with SSTR2 and SSTR5. Considering SSTR2, an interesting change in the binding energy of SST with SSTR2 was detected in the L13P mutant form. This observation attributed to the vital involvement of this amino acid substitution in inducing conformational alteration in the signal peptide region within the SST with a series of undesired consequences in terms of binding with SSTR2. Noteworthy, SSTR2 is responsible for inhibiting the secretion of pancreatic enzymes upon binding with SST.[61] Hence, such downstream inhibition might be exposed to disturbance as a consequence of this aberrant binding between L13P and SSTR2. Interestingly, the signal peptide was reported to be involved in directing and sorting SST to the endoplasmic reticulum after being synthesized,[62] which entails a disruption of both processes in the case of L13P mutation. However, this interesting conversion induced by L13P was not seen in the G104S mutation. Meanwhile, both SNPs induced substantial conversions in the binding activity with SSTR5 by inducing conformational changes in SST. This altered SST-SSRT5 binding may be associated with subsequent alteration in SSTR5, which has been reported to inhibits adenylyl cyclase, activate mitogen-activated protein kinase cascade, and mediates antiproliferative action of somatostatin in tumor cells.[63] The somatostatin-14 domain has widely been accepted to be involved in the binding with several SSTRs molecules.[64] So, both nsSNPs have been shown to exhibit obvious alterations in the binding with receptors, which cause several damaging effects on the SST-mediated cellular hormonal regulation.

Whatever the pattern each deleterious nsSNP takes in the disruption of SST activity, one or more of the SST-mediated biological processes would be disrupted, such as the negative proliferation of cell proliferation,[65] response to nutrients,[2] response to heat, metabolic regulation of growth hormone,[66] neurotransmission control,[67] G-protein coupled receptor protein signaling,[68] and other signal transduction activities.[69] As well, the implication of dysfunctional SST has also been reported in several syndromes, such as schizophrenia, depression, Alzheimer's disease, and bipolar disorder.[70] Thus, the possible pathogenic outcomes of such amino acid substitutions deserve more attention in clinical investigations. Due to the confirmed ability of these missense SNPs to persuade dramatic alterations in SST architecture and its subsequent binding with some SSTRs, it can be stated that such altered complexes seem to disrupt the consequent cascades of the hormonal pathway(s) in which SST is involved.

Conclusion

This study observed two highly deleterious nsSNPs in SST as revealed by 20 state-of-the-art *in silico* tools whether based on a primary FASTA sequence or the tertiary PDB structure. Both L13P and G104S risky nsSNPs exhibited variable conformational alterations in the binding of SST with two of its receptors, SSTR2 and SSTR5. Consequently, the presented inclusive data explained the precise role of both highly damaging missense SNPs in the disruption of the SST conformation. This study gives an in-depth interpretation for clinicians to assess the SST-linked syndromes by knowing the type, grade, and severity consequences of each deposited nsSNP on SST protein. Hence, comprehensive clinical-based investigations are required on a large-scale population to characterize these data for the validation of the findings.

Conflict of Interest Disclosures

The authors declare that they have no conflicts interest.

Acknowledgment

The author declares that this work was not receiving any fund from any institution or agency.

References

1. Stueven AK, Kayser A, Wetz C, Amthauer H, Wree A, Tacke F, et al. Somatostatin analogues in the treatment of neuroendocrine tumors: past, present and future. Int J Mol Sci. 2019;20(12):3049. doi:10.3390/ijms20123049
2. Schusdziarra V. The physiological role of somatostatin in the regulation of nutrient homeostasis. In: Somatostatin. Springer, Berlin, Heidelberg; 1992. p. 43-54. doi:10.1007/978-3-642-76948-1_4
3. Morisset J. Somatostatin: one of the rare multifunctional inhibitors of mammalian species. Pancreas. 2017;46(1):8-18. doi:10.1097/MPA.0000000000000716
4. Thomas RP, Hellmich MR, Townsend Jr CM, Evers BM. Role of gastrointestinal hormones in the proliferation of normal and neoplastic tissues. Endocr Rev. 2003;24(5):571-99. doi:10.1210/er.2002-0028
5. Al-Hindy HA, Mousa MJ, Shaker AK. No significant relationship of ferritin levels to the levels of platelet-derived growth factor (PDGF) in the peripheral blood of transfusion-dependent β-thalassemia major patients with growth retardation. Int J Pharm Res. 2020;12(3):568-75. doi:10.31838/ijpr/2020.12.03.084
6. Eigler T, Ben-Shlomo A. Somatostatin system: molecular mechanisms regulating anterior pituitary hormones. J Mol Endocrinol. 2014;53(1):R1-19.
7. Israʌl M. A possible primary cause of cancer: deficient cellular interactions in endocrine pancreas. Mol Cancer. 2012;11(1):63. doi:10.1186/1476-4598-11-63
8. Leiszter K, Sipos F, Galamb O, Krenacs T, Veres G, Wichmann B, et al. Promoter hypermethylation-related reduced somatostatin production promotes uncontrolled cell proliferation in colorectal cancer. PLoS One. 2015;10(2):e0118332.

doi:10.1371/journal.pone.0118332
9. Friedewald WT, Levy RI, Fredrickson DS. Estimation of the concentration of low-density lipoprotein cholesterol in plasma, without use of the preparative ultracentrifuge. Clin Chem. 1972;18(6):499-502. doi:10.1093/clinchem/18.6.499
10. Hedback T, Almgren P, Nilsson PM, Melander O. N-terminal prosomatostatin as a risk marker for cardiovascular disease and diabetes in a general population. J Clin Endocrinol Metab. 2016;101(9):3437-44. doi:10.1210/jc.2016-1736
11. Tremblay M, Brisson D, Gaudet D. Association between a polymorphic poly-T repeat sequence in the promoter of the somatostatin gene and hypertension. Hypertens Res. 2016;39(6):467-74. doi:10.1038/hr.2016.4
12. Hashim HO, Al-Saadi AH, Haider AH, Zaidan HK. Association of Uromodulin rs13333226 and Angiotensinogen rs699 genes variants with essential hypertension in Arab Iraqis of Babylon province. Res J Pharm Biol Chem Sci. 2015;6(6):589-601.
13. Holm H, Nagga K, Nilsson ED, Ricci F, Cinosi E, Melander O, et al. N-terminal prosomatostatin and risk of vascular dementia. Cerebrovasc Dis. 2017;44(5-6):259-65. doi:10.1159/000479940
14. Lambert GA, Zagami AS. Does somatostatin have a role to play in migraine headache?. Neuropeptides. 2018;69:1-8. doi:10.1016/j.npep.2018.04.006
15. Gunther T, Tulipano G, Dournaud P, Bousquet C, Csaba Z, Kreienkamp HJ, et al. International Union of Basic and Clinical Pharmacology. CV. Somatostatin receptors: structure, function, ligands, and new nomenclature. Pharmacol Rev. 2018;70(4):763-835. doi:10.1124/pr.117.015388
16. Al-Shuhaib MB, Al-Shuhaib JM. Integrating state-of-the-art *in silico* tools with molecular docking to predict the impact of the most deleterious amino acid substitutions on TRAPPC6A protein. Curr Sci. 2021;120(2):398-405. doi:10.18520/cs/v120/i2/398-405
17. Al-Shuhaib MB. The Deleterious F109S Mutation Disrupts Binding of Sex-Determining Region Y with DNA. Karbala Int J Mod Sci. 2020;6(4):385-95. doi:10.33640/2405-609X.2082
18. Prabhu BN, Kanchamreddy SH, Sharma AR, Bhat SK, Bhat PV, Kabekkodu SP, et al. Conceptualization of functional single nucleotide polymorphisms of polycystic ovarian syndrome genes: an *in silico* approach. J Endocrinol Invest. 2021;44(8):1783-93. doi:10.1007/s40618-021-01498-4
19. Ng PC, Henikoff S. Predicting the effects of amino acid substitutions on protein function. Annu Rev Genomics Hum Genet. 2006;7:61-80. doi:10.1146/annurev.genom.7.080505.115630
20. Adzhubei I, Jordan DM, Sunyaev SR. Predicting functional effect of human missense mutations using PolyPhen-2. Curr Prot Hum Genet. 2013;76(1):7-20. doi:10.1002/0471142905.hg0720s76
21. Ioannidis NM, Rothstein JH, Pejaver V, Middha S, McDonnell SK, Baheti S, et al. REVEL: an ensemble method for predicting the pathogenicity of rare missense variants. Am J Hum Genet. 2016;99(4):877-85. doi:10.1016/j.ajhg.2016.08.016
22. Choi Y, Sims GE, Murphy S, Miller JR, Chan AP. Predicting the functional effect of amino acid substitutions and indels. PloS One. 2012;7(10):e46688 doi:10.1371/journal.pone.0046688
23. Tang H, Thomas PD. PANTHER-PSEP: predicting disease-causing genetic variants using position-specific evolutionary preservation. Bioinformatics. 2016;32(14):2230-2. doi:10.1093/bioinformatics/btw222
24. Smigielski EM, Sirotkin K, Ward M, Sherry ST. dbSNP: a database of single nucleotide polymorphisms. Nucleic Acids Res. 2000;28(1):352-5. doi:10.1093/nar/28.1.352
25. Capriotti E, Calabrese R, Casadio R. Predicting the insurgence of human genetic diseases associated to single point protein mutations with support vector machines and evolutionary information. Bioinformatics. 2006;22(22):2729-34. doi:10.1093/bioinformatics/btl423
26. Reva B, Antipin Y, Sander C. Predicting the functional impact of protein mutations: application to cancer genomics. Nucleic Acids Res. 2011;39(17):e118. doi:10.1093/nar/gkr407
27. Yates CM, Filippis I, Kelley LA, Sternberg MJ. SuSPect: enhanced prediction of single amino acid variant (SAV) phenotype using network features. J Mol Biol. 2014;426(14):2692-701. doi:10.1016/j.jmb.2014.04.026
28. Salgado D, Desvignes JP, Rai G, Blanchard A, Miltgen M, Pinard A, et al. UMD-predictor: a high-throughput sequencing compliant system for pathogenicity prediction of any human cDNA substitution. Hum Mut. 2016;37(5):439-46. doi:10.1002/humu.22965
29. Waterhouse A, Bertoni M, Bienert S, Studer G, Tauriello G, Gumienny R, et al. SWISS-MODEL: homology modelling of protein structures and complexes. Nucleic Acids Res. 2018;46(W1):W296-303. doi:10.1093/nar/gky427
30. Laskowski RA, MacArthur MW, Thornton JM. PROCHECK: validation of protein-structure coordinates. In Rossmann MG, and Arnold E (eds), International Tables of Crystallography. 2006; Vol. F. ch. 25.2, pp. 722-5.
31. Capriotti E, Fariselli P, Casadio R. I-Mutant2.0: predicting stability changes upon mutation from the protein sequence or structure. Nucleic Acids Res. 2005;33(suppl_2):W306-10. doi:10.1093/nar/gki375
32. Laimer J, Hofer H, Fritz M, Wegenkittl S, Lackner P. MAESTRO-multi agent stability prediction upon point mutations. BMC bioinform. 2015;16(1):116. doi:10.1186/s12859-015-0548-6
33. Quan L, Lv Q, Zhang Y. STRUM: structure-based prediction of protein stability changes upon single-point mutation. Bioinformatics. 2016;32(19):2936-46. doi:10.1093/bioinformatics/btw361
34. Cheng J, Randall A, Baldi P. Prediction of protein stability changes for single-site mutations using support vector machines. Proteins: Struct Funct Genet. 2006;62(4):1125-32. doi:10.1002/prot.20810
35. Chen CW, Lin J, Chu YW. iStable: off-the-shelf predictor integration for predicting protein stability changes. BMC bioinformatics 2013;14:S5. doi:10.1186/1471-2105-14-S2-S5
36. Parthiban V, Gromiha MM, Schomburg D. CUPSAT: prediction of protein stability upon point mutations. Nucleic Acids Res. 2006;34(suppl_2):W239-42. doi:10.1093/nar/gkl190
37. Rodrigues CH, Pires DE, Ascher DB. DynaMut: predicting the impact of mutations on protein conformation, flexibility and stability. Nucleic Acids Res. 2018;46(W1):W350-5. doi:10.1093/nar/gky300
38. Worth CL, Preissner R, Blundell TL. SDM—a server for predicting effects of mutations on protein stability and malfunction. Nucleic Acids Res. 2011;39(suppl_2):W215-22. doi:10.1093/nar/gkr363
39. Pires DE, Ascher DB, Blundell TL. DUET: a server for predicting effects of mutations on protein stability using an integrated computational approach. Nucleic Acids Res. 2014;42(W1):W314-9. doi:10.1093/nar/gku411
40. Kallberg M, Wang H, Wang S, Peng J, Wang Z, Lu H, et al. Template-based protein structure modeling using the RaptorX web server. Nat Protoc. 2012;7(8):1511-22.

doi:10.1038/nprot.2012.085
41. Wu Q, Peng Z, Zhang Y, Yang J. COACH-D: improved protein–ligand binding sites prediction with refined ligand-binding poses through molecular docking. Nucleic Acids Res. 2018;46(W1):W438-42. doi:10.1093/nar/gky439
42. Zhang Y, Skolnick J. TM-align: a protein structure alignment algorithm based on the TM-score. Nucleic Acids Res. 2005;33(7):2302-9. doi:10.1093/nar/gki524
43. Zhang C, Freddolino PL, Zhang Y. COFACTOR: improved protein function prediction by combining structure, sequence and protein–protein interaction information. Nucleic Acids Res. 2017;45(W1):W291-9. doi:10.1093/nar/gkx366
44. Brylinski M, Skolnick J. A threading-based method (FINDSITE) for ligand-binding site prediction and functional annotation. Proc Natl Acad Sci U S A. 2008;105(1):129-34. doi:10.1073/pnas.0707684105
45. Capra JA, Laskowski RA, Thornton JM, Singh M, Funkhouser TA. Predicting protein ligand binding sites by combining evolutionary sequence conservation and 3D structure. PLoS Comput Biol. 2009;5(12):e1000585. doi:10.1371/journal.pcbi.1000585
46. Ashkenazy H, Erez E, Martz E, Pupko T, Ben-Tal N. ConSurf 2010: calculating evolutionary conservation in sequence and structure of proteins and nucleic acids. Nucleic Acids Res. 2010;38(suppl_2):W529-33. doi:10.1093/nar/gkq399
47. Johansson MU, Zoete V, Michielin O, Guex N. Defining and searching for structural motifs using DeepView/Swiss-PdbViewer. BMC bioinform. 2012;13(1):173. doi:10.1186/1471-2105-13-173
48. Krissinel E, Henrick K. Secondary-structure matching (SSM), a new tool for fast protein structure alignment in three dimensions. Acta Crystallogr D Biol Crystallogr. 2004;60(12):2256-68. doi:10.1107/S0907444904026460
49. van Gunsteren WF, Billeter SR, Eising AA, Hunenberger PH, Kruger PK, Mark AE, et al. Biomolecular simulation: the GROMOS96 manual and user guide. Vdf Hochschulverlag AG an der ETH Zurich, Zurich. 1996;86:1-044.
50. Kuriata A, Gierut AM, Oleniecki T, Ciemny MP, Kolinski A, Kurcinski M, et al. CABS-flex 2.0: a web server for fast simulations of flexibility of protein structures. Nucleic Acids Res. 2018;46(W1):W338-43. doi:10.1093/nar/gky356
51. Phillips JC, Hardy DJ, Maia JD, Stone JE, Ribeiro JV, Bernardi RC, et al. Scalable molecular dynamics on CPU and GPU architectures with NAMD. J Chem Phys. 2020;153(4):044130. doi:10.1063/5.0014475
52. Jo S, Kim T, Iyer VG, Im W. CHARMM-GUI: a web-based graphical user interface for CHARMM. J Comput Chem. 2008;29(11):1859-65. doi:10.1002/jcc.20945
53. Boonstra S, Onck PR, van der Giessen E. CHARMM TIP3P water model suppresses peptide folding by solvating the unfolded state. J Phys Chem B. 2016;120(15):3692-8. doi:10.1021/acs.jpcb.6b01316
54. Humphrey W, Dalke A, Schulten K. VMD: visual molecular dynamics. J Mol Graph. 1996;14(1):33-8. doi:10.1016/0263-7855(96)00018-5
55. Szklarczyk D, Franceschini A, Wyder S, Forslund K, Heller D, Huerta-Cepas J, et al. STRING v10: protein–protein interaction networks, integrated over the tree of life. Nucleic Acids Res. 2015;43(D1):D447-52. doi:10.1093/nar/gku1003
56. Van Zundert GC, Rodrigues JP, Trellet M, Schmitz C, Kastritis PL, Karaca E, et al. The HADDOCK2. 2 web server: user-friendly integrative modeling of biomolecular complexes. J Mol Biol. 2016;428(4):720-5. doi:10.1016/j.jmb.2015.09.014
57. Qin S, Zhou HX. meta-PPISP: a meta web server for protein-protein interaction site prediction. Bioinformatics. 2007;23(24):3386-7. doi:10.1093/bioinformatics/btm434
58. Al-Shuhaib MB. D76V, L161R, and C117S are the most pathogenic amino acid substitutions with several dangerous consequences on leptin structure, function, and stability. Egypt J Med Hum Genet. 2019;20(1):32. doi:10.1186/s43042-019-0033-2
59. Arifuzzaman M, Mitra S, Das R, Hamza A, Absar N, Dash R. *In silico* analysis of nonsynonymous single-nucleotide polymorphisms (nsSNPs) of the SMPX gene. Ann Hum Genet. 2020;84(1):54-71. doi:10.1111/ahg.12350
60. AbdulAzeez S, Borgio JF. *In-silico* computing of the most deleterious nsSNPs in HBA1 gene. PloS One. 2016;11(1):e0147702. doi:10.1371/journal.pone.0147702
61. Kailey B, van de Bunt M, Cheley S, Johnson PR, MacDonald PE, Gloyn AL, Rorsman P, Braun M. SSTR2 is the functionally dominant somatostatin receptor in human pancreatic β-and α-cells. Am J Physiol - Endocrinol Metab. 2012;303(9):E1107-16. doi:10.1152/ajpendo.00207.2012
62. Davies JS, Holter JL, Knight D, Beaucourt SM, Murphy D, Carter DA, et al. Manipulating sorting signals to generate co-expression of somatostatin and eGFP in the regulated secretory pathway from a monocistronic construct. J Mol Endocrinol. 2004;33(2):523-32. doi:10.1677/jme.1.01578
63. Shenoy PA, Kuo A, Khan N, Gorham L, Nicholson JR, Corradini L, et al. The somatostatin receptor-4 agonist J-2156 alleviates mechanical hypersensitivity in a rat model of breast cancer induced bone pain. Front Pharmacol. 2018;9:495. doi:10.3389/fphar.2018.00495
64. Corness JD, Demchyshyn LL, Seeman P, Van Tol HH, Srikant CB, Kent G, et al. A human somatostatin receptor (SSTR3), located on chromosome 22, displays preferential affinity for somatostatin-14 like peptides. FEBS Lett. 1993;321(2-3):279-84. doi:10.1016/0014-5793(93)80124-D
65. Florio T, Schettini G. Somatostatin and its receptors. Role in the control of cell proliferation. Minerva Endocrinol. 2001;26(3):91-102.
66. Koutkia P, Canavan B, Breu J, Johnson ML, Grinspoon SK. Nocturnal ghrelin pulsatility and response to growth hormone secretagogues in healthy men. Am J Physiol - Endocrinol Metab. 2004;287(3):E506-12. doi:10.1152/ajpendo.00548.2003
67. Stengel A, Tache Y. Activation of somatostatin 2 receptors in the brain and the periphery induces opposite changes in circulating ghrelin levels: functional implications. Front Edocrinol. 2013;3:178. doi:10.3389/fendo.2012.00178
68. Egerod KL, Engelstoft MS, Lund ML, Grunddal KV, Zhao M, Barir-Jensen D, et al. Transcriptional and functional characterization of the G protein-coupled receptor repertoire of gastric somatostatin cells. Endocrinology. 2015;156(11):3909-23. doi:10.1210/EN.2015-1388
69. Ferjoux G, Bousquet C, Cordelier P, Benali N, Lopez F, Rochaix P, et al. Signal transduction of somatostatin receptors negatively controlling cell proliferation. J Physiol Paris. 2000;94(3-4):205-10. doi:10.1016/S0928-4257(00)00206-0
70. Liguz-Lecznar M, Urban-Ciecko J, Kossut M. Somatostatin and somatostatin-containing neurons in shaping neuronal activity and plasticity. Front Neural Circuits. 2016;10:48. doi:10.3389/fncir.2016.00048